Int J Clin Exp Med 2025;18(9):243-254
www.ijcem.com /ISSN:1940-5901/IJCEM0164366

Original Article

Myocardial structural alterations induced by amitriptyline and paroxetine in a rat model of menopause: a histomorphometric and immunohistochemical study

Emel Kurtoglu Ozdes[1], Berrin Zuhal Altunkaynak[2], Burcu Delibas[3], Taskin Ozdes[4], Suleyman Kaplan[5]

[1]Department of Obstetrics and Gynecology, Faculty of Medicine, Kirklareli University, Kirklareli, Türkiye; [2]Department of Histology and Embryology, Faculty of Medicine, Okan University, Istanbul, Türkiye; [3]Department of Histology and Embryology, Faculty of Medicine, Recep Tayyip Erdogan University, Rize, Türkiye; [4]Department of Forensic Medicine, Faculty of Medicine, Kirklareli University, Kirklareli, Türkiye; [5]Department of Histology and Embryology, Faculty of Medicine, Ondokuz Mayis University, Samsun, Türkiye

Received March 6, 2025; Accepted September 4, 2025; Epub September 15, 2025; Published September 30, 2025

Abstract: Objective: This study aimed to investigate the effects of amitriptyline (AMI) and paroxetine (PRO) on the histo-morphometrical structure of the heart in an ovariectomized (OVX) rat model. Methods: Twenty-four female, adult Sprague Dawley rats were randomly divided to four groups (n=6). While Group 1 was used as the control, rats in Groups 2, 3 and 4 were exposed to bilateral ovariectomy 7 days before the drug treatment. AMI and PRO were given to animals in groups 2, 3 and 4. Following drug administration for 28 days, the hearts of the rats were removed and the heart volume, interstitial tissue and micro-vessels, as well as the number of cardiac myocytes were evaluated by using the Cavalieri principle and physical dissection methods; histological structure was evaluated under a light microscope and immunohistochemical staining for C-Fos and NF-kB antibodies were performed. Results: PRO caused to increase in the volume of the heart and connective tissue. AMI led to increase in the volume of the micro vessels. PRO and especially AMI ameliorate the decreased number of the cardiac myocytes due to OVX. The histological architecture of myocardium was corrupted in AMI and especially PRO treated groups. Also, AMI and PRO induced C-Fos and NF-kb immunoreactivity following OVX procedures in rats. Conclusion: Our study shows that AMI and PRO induce myocardial abnormalities and damage cardiac myocytes. Therefore, clinicians should make treatment decisions on a case-by-case basis, considering the detailed anamnesis of each patient with post-menopausal depression.

Keywords: Amitriptyline, anti-depressant therapy, heart, immunohistochemistry, paroxetine, postmenopausal depression

Introduction

Depression is a major health problem worldwide, and it is extremely common in women of all age groups. Among the female-specific reproductive events related to mood disorders, the menopausal period is marked by an increased risk of anxiety and depression. Several studies have identified sex hormonal changes affecting the neurochemical pathways related to depression, but no definitive conclusions have been drawn [1, 2]. Furthermore, there have been numerous studies suggesting significant associations of demographic and psychosocial features, such as poor sleep, vasomotor symptoms, education, stress, and smoking, with menopausal depression, but the evidence is inconsistent or lacking [3]. The issue of menopausal depression is highly important due to the increased risk of associated problems, such as cardiovascular disease, sudden cardiac death, and suicide [4, 5]. The declined level of estrogen, which has anti-inflammatory and cardio-protective effects during the menopausal period, with increased sympathetic and decreased parasympathetic activation, the pro-inflammatory response of menopausal depression contributes to an increased cardiovascular risk accumulation [6, 7].

Since depression is a challenging condition for most postmenopausal women, antidepressant

drugs alone or combined with hormonal therapy can be considered for menopausal depression and other related problems, including vasomotor symptoms and insomnia despite reported increased risk of some systemic diseases such as cardiovascular disease. Among these medications, selective serotonin reuptake inhibitors (SSRIs) are first-line treatments as they are believed to be safe and effective. However, studies have reported possible adverse cardiovascular effects, including increased risk of myocardial infarction in people aged 65 and over, elevation of blood pressure, QT interval prolongation, and arrhythmia [8-10].

Previous immunohistochemical research regarding C-Fos proto-oncogene expression, which participates in a variety of physiological processes, including signal transduction and plasticity of the nervous system, has also been found to be induced in cardiac cells in response to stimuli, such as viral infection, norepinephrine administration, immobilization, emotional stress, or ischemia-reperfusion, most of which are present in postmenopausal depression [11-13]. Additionally, activation of NF-kB signaling is important in the acute response to hypoxia and reperfusion injury, while prolonged activation is detrimental to the heart. A recent report demonstrated that NF-kB signaling plays a pivotal role in arrhythmogenic cardiomyopathy (ACM), which is an inherited disease that can cause sudden death [14]. In previous research, researchers have reported that nuclear factor-kappa B (NF-kB) signaling functions in myocardial remodeling by regulating inflammation and cell death [15]. Interestingly, short-term activation of NF-kB has a cardioprotective effect against hypoxia and reperfusion injury, while elongated activation promotes heart failure due to excessive inflammation. In the therapy of the post-menopausal depression, tricyclic antidepressants (TCAs) can be recommended to women with menopausal depression who cannot use SSRIs due to side effects. However, it should be mentioned that adverse effects, such as arrhythmia and bundle branch block, have been reported in some studies, while others report safety [16, 17]. Although there have been several studies regarding the effects of TCAs and SSRIs on the cardiovascular system in women with depression; there is no study comparing their effects on the heart structure and morphology and clarifying the effect mechanism in the light of the molecular findings like immunohistochemical data.

Therefore, the purpose of this study was to investigate the cellular effects of Paroxetine (PRO), which is one of the first lines of prescribed SSRIs drugs, and amitriptyline (AMI), which is another widely prescribed TCA drug for the heart, using Cavalieri's principle and physical dissection methods, as well as immunohistochemistry analyses of NF-kB and C-Fos expressions in the heart for the first time. We aim to find the relation between the possible affect mechanism of the drugs and the reorganization process of the cardiac myocytes in terms of the inflammatory pathways and cellular activity following the anti-depressant therapy in post-menopausal depression.

Material and methods

Animals and experimental protocol

This experiment utilized twenty-four female Sprague Dawley rats, aged 9-10 weeks, with a weight range of 250-300 g. All animal experiments were conducted in accordance with the ethical guidelines and regulations set forth by the Ondokuz Mayıs University Ethics Committee for Animal Experiments (OMÜ-HADYEK). The experimental procedures described in this study were reviewed and approved by the committee under protocol number [2014/02]. All animals were obtained from the Experimental Animal Research and Application Center of Ondokuz Mayıs University and were housed, handled, and treated in accordance with national and institutional guidelines for the care and use of laboratory animals. The rats were placed in standard laboratory conditions (22 ± 1°C, 12-hour light/dark cycle) and provided with food at the Ondokuz Mayis University Experimental Animal Production and Research Center, after obtaining authorization. Both tap water and ordinary rat food were supplied. Following a one-week acclimation period, the animals were randomly divided into four equal groups. The control animals, totaling six, were assigned to the first group and were not subjected to any experimental procedures. Eighteen rats underwent a bilateral ovariectomy (OVX) surgery, with each in one of the three groups consisting of six rats each. The rats were anesthetized by intraperitoneal (i.p.) administration of 100 mg/kg ketamine and 0.75

mg/kg chlorpromazine for this procedure. The ovaries were removed following a surgical procedure in which a 0.5-1 cm incision was created along the midline of the lower abdomen. After a week of recovery, the rats were subjected to the following medication administration protocol: 1. Control Group: Consisted six healthy animals that did not receive any specific treatment for 28 days. 2. Group 2 (OVX Group): Six animals were given 1 ml of distilled water through the abdominal cavity every day for 28 days following the healing period. 3. Group 3 (AMI Group): Six OVX animals were given a daily intraperitoneal injection of 10 mg/1 ml AMI from Sigma-Aldrich Chemical Co. (St. Louis, Missouri, USA) for 28 days following the healing period. 4. Group 4 (PRO Group): Comprised of OVX animals who were administered a daily intraperitoneal injection of 10 mg/1 ml PRO for 28 days following the healing period. The PRO was supplied by the Ali Raif Pharmaceutical Company located in Istanbul, Türkiye.

Following the 28-day experiment, at the end of the experiment, animals were deeply anesthetized with an intraperitoneal injection of ketamine (80-100 mg/kg) and xylazine (10-15 mg/kg). The depth of anesthesia was confirmed by the absence of pedal withdrawal and corneal reflexes. Once a surgical plane of anesthesia was reached, a thoracotomy was performed to expose the heart. Trans-cardiac perfusion was then carried out by inserting a cannula into the left ventricle. The right atrium was incised to allow efflux. Perfusion was initiated with cold phosphate-buffered saline (PBS, pH 7.4) for approximately 5 minutes to flush out the blood, followed by cold 4% paraformaldehyde (PFA) in PBS for 10-15 minutes to achieve tissue fixation. As a result of the perfusion procedure, the animals were considered deceased by exsanguination. Then, hearts were carefully excised, post-fixed in 4% PFA at 4°C for 24 hours, and then transferred to a 30% sucrose solution in PBS for cryoprotection prior to embedding and sectioning. All efforts were made to minimize animal suffering and reduce the number of animals used in accordance with the principles of the 3Rs (Replacement, Reduction, Refinement).

Routine tissue process for light microscopy

Tissue processing for stereological and light microscopic studies includes the meticulous preparation of biological samples for inspection utilizing sophisticated techniques and state-of-the-art equipment.

The removed hearts were placed in a solution of 10% phosphate buffered formalin for duration of 48-55 hours. Afterwards, they underwent a sequence of graded alcohol and xylol solutions prior to being embedded in paraffin. The blocks were sliced into serial sections with a thickness of 5 μm using a Leica RM2125RT microtome (Leica Microsystems in Istanbul, Türkiye). The sections were stained with Hematoxylin-eosin for conventional histological examination, Masson's thrichrome was used for assessment of connective tissue and collagen fiber levels, and C-Fos and NF-Kb antibodies for targeted analyses of specific regions. The sections were evaluated using stereological and immunohistochemical techniques, with observations conducted under a light microscope (Olympus BX43; Tokyo, Japan). All images for histochemical and stereological analyses were taken by ×4 and ×40 objectives for general structural view and details of the heart, respectively. Moreover, ocular and camera magnifications were ×10, additionally.

Stereological analysis

The volumes of the heart, connective tissue, and micro-vessels: The unbiased Cavalieri principle was applied to microscopic images to estimate the total volume of cardiac components using the point-counting technique [18]. This method involves the random placement of a point-counting grid on tissue sections prepared through systematic random sampling. Points intersecting the regions of interest are counted, and the surface area is calculated by multiplying the number of intersecting points by the area represented by each point, based on the known grid point size.

An appropriate point density for the counting grid was determined to ensure acceptable levels of the coefficient of error (CE) and coefficient of variation (CV) for the regions of interest. The volumetric measurements of cardiac components such as the myocardium, endocardium, epicardium, and total heart volume (ΣV) were calculated using the following formula:

$$\Sigma V = t \cdot \Sigma A \Sigma V = t \cdot \Sigma A.$$

Here, t represents the total thickness of the sampled sections (including the interval betwe-

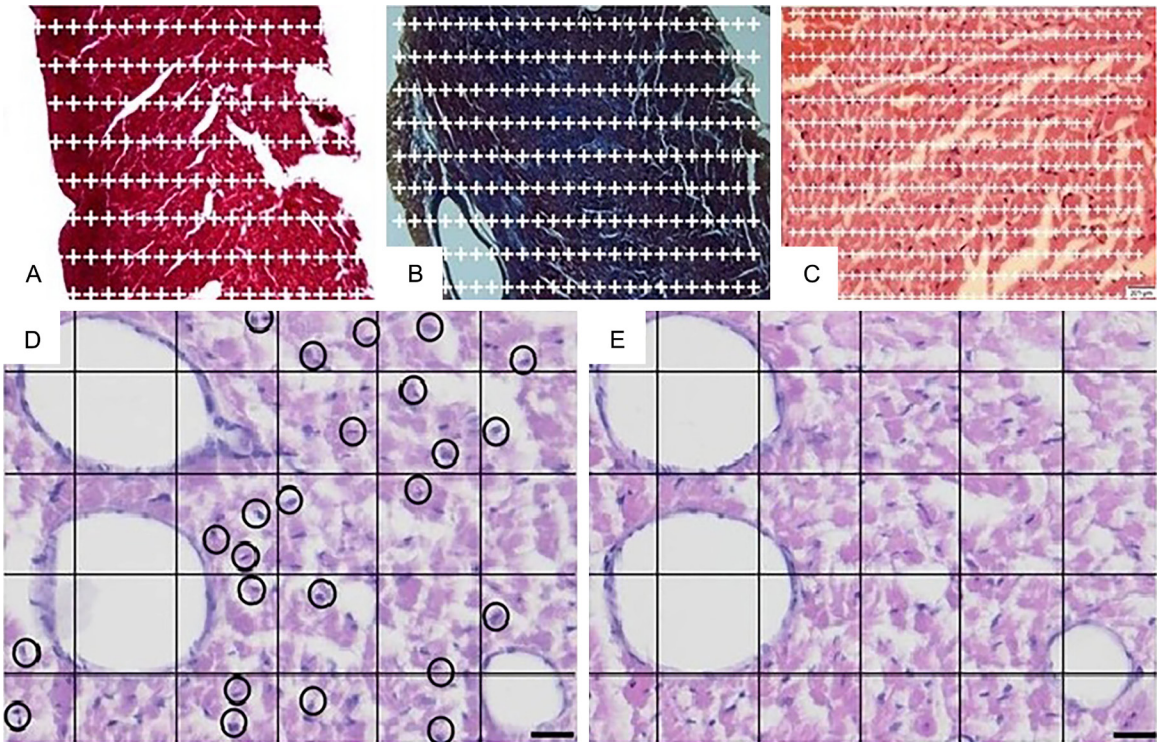

Figure 1. The views of the heart sections, the sections are superimposed point counting grids for estimating the cardiac volume (A), interstitial tissue volume (B) and micro-vessel volume, respectively (C) location of the grid in order to calculate the heart wall (Scale bar is 200 μm). In (D and E), the same area is seen in two adjacent sections, separated by 5 μm, respectively. (D) Reference section, (E) look-up section. Nuclei located inside the circle in (D) were considered as dissection particles if their profiles are not seen in the look-up section (E). Scale bar is 50 μm.

en them), and ΣA is the total cross-sectional area of the cardiac tissue of interest. This area is calculated using:

$$\Sigma A = a(p) \cdot \Sigma P \Sigma A = a(p) \cdot \Sigma P.$$

In this formula, a(p) is the area associated with each point on the grid, and ΣP is the total number of points that intersect the target cardiac regions in the sections.

Quantification of cardiac myocytes

The selection of the physical dissector pairings was conducted following the methods established by Sterio in 1894. Based on data obtained from an initial investigation, pairings were chosen randomly from every 5th section. As a result of this approach, around 15-20 pairs of sections were generated, which were subsequently examined. Dissection pairs were systematically taken from the tissue at regular intervals until the entire tissue sample was depleted. Each slide consisted of two consecutive segments. The digital camera captured images of neighboring sections at a magnification of ×400. The nuclei of myocytes that were observable in the reference section but not in the look-up area were counted. To increase the quantity of measurable particles, such as nuclei, we altered the operation of sections in the second stage. An unbiased counting frame was placed on both the reference and lookup sections of the computer screen to perform counting utilizing the dissector counting method. The lower and left borders of the counting frame are identified as the forbidden (exclusion) lines, along with the extension lines. The remaining edges of the frame, as well as the upper-right corner, were identified as inclusion sites. Any particle that came into contact with these lines or was located within the frame was documented as a dissector particle [18] (Refer to **Figure 1**, specifically **Figure 1D**, **1E**). The dimensions of the unbiased counting device were adjusted to include approximately 600 myocytes from each specimen. The dimensions of

Table 1. Assignment of immunohistochemical score according to staining intensity and percentage of positively stained cardiomyocytes

Score	*Positive cell (%)*	*Intensity*
0	0-15	Negative
1	16-30	Weak positive
2	30-60	Moderate positive
3	> 61	Strong positive

the counting frame depicted on the PC screen in this investigation were 10 cm × 10 cm. The precise measurements of the counting frame, which were 6.250×10^{-5} cm^2, were determined using a specific mathematical formula:

The real dimension is calculated by dividing the screen size of the frame by the total magnification of the microscope. The given method was employed to quantify the average numerical density (NV) of cardiac myocytes (CM), represented as Nv (CM), per cubic millimeter (mm^3). The formula for net volume flow rate (Nv) in terms of cumulative mass flow rate (CM), time (t), and cross-sectional area (A) is given by:

$Nv(CM)=\Sigma Q\text{-}(CM)/t\cdot A.$

The equation calculates ΣQ-myocyte, which corresponds to the total count of nuclei observed in the reference section. The average thickness of the section, which is 5 μm, is represented by the variable t. The area of the counting frame without any bias is designated by A.

The equation was utilized to approximate the overall quantity of cardiac myocytes (TN (CM)) in the rat heart is as follows: The total number of cases (TN) in a certain country is equal to the number of new cases (Nv) in that country multiplied by the case velocity (CV). The abbreviation "Nv(CM)" denotes the numerical density of cardiac myocytes in cubic millimeters (mm^3), while "CV" signifies the heart volume measured through the application of the Cavalieri principle.

Immunohistochemistry

Immunohistochemical assays were performed to evaluate the expression of the C-Fos protein in 5-μm sections obtained from each animal. The deparaffinization and rehydration operations were performed accurately utilizing a series of alcohol and xylene solvents. The staining method was performed using an HRP/AEC detection IHC kit (Catalog Number: ab97-080, Abcam, Istanbul, Türkiye). Prior to immunostaining, the slices underwent incubation at 650 W for 10 minutes in citrate buffer (pH 6.0) to enhance epitope recovery. The immunohistochemical labeling was performed using a primary mouse monoclonal antibody that specifically targets C-Fos (CN: SAB5700610, Sigma; Istanbul, Türkiye) and NF-kB (for P65 domain CN: ab16502, Abcam, Istanbul, Türkiye) antibodies. The antibodies were diluted in antibody diluents at a ratio of 1:250. The specimens underwent overnight treatment at a temperature of 4°C. After being washed three times with phosphate buffer (pH 7.4), the sections were treated with a peroxidase-labeled dextran polymer that was linked to goat anti-mouse and anti-rabbit immunoglobulins. The color was produced using Diamidine-2'-phenylindole dihydrochloride (DAPI, Sigma Aldrich; Istanbul, Türkiye). Mayer's hematoxylin was used as a counterstain, and Kaiser's glycerol gelatin from Merck AG in Istanbul, Türkiye, was used to mount the cover slips. The stained slices were analyzed using light microscopy. An analysis was conducted on the tissues to ascertain the existence of antibodies that bind to the cellular and matrix components. The immunohistochemistry score was adapted from the previous study reported by Ceccarelli et al. [19], positively stained cells were quantified using NIH ImageJ Software (version 2; National Institutes of Health, Bethesda, MD). Staining intensity of the cells was assessed on a scale from 0 to 3: a score of 0 was assigned to completely negative samples, while weak, moderate, and strong staining corresponded to scores of 1, 2, and 3, respectively. The final immunohistochemical (IHC) score for each sample group was calculated by multiplying the staining intensity score by the percentage of the positive stained cells. Based on the final score, samples were categorized into four groups: negative, weakly positive, moderately positive, and strongly positive (see **Table 1**).

Statistical analysis

The data obtained was subjected to statistical analysis using Microsoft® SPSS version 21.0 for Windows (SPSS, Inc., Chicago, Illinois, USA).

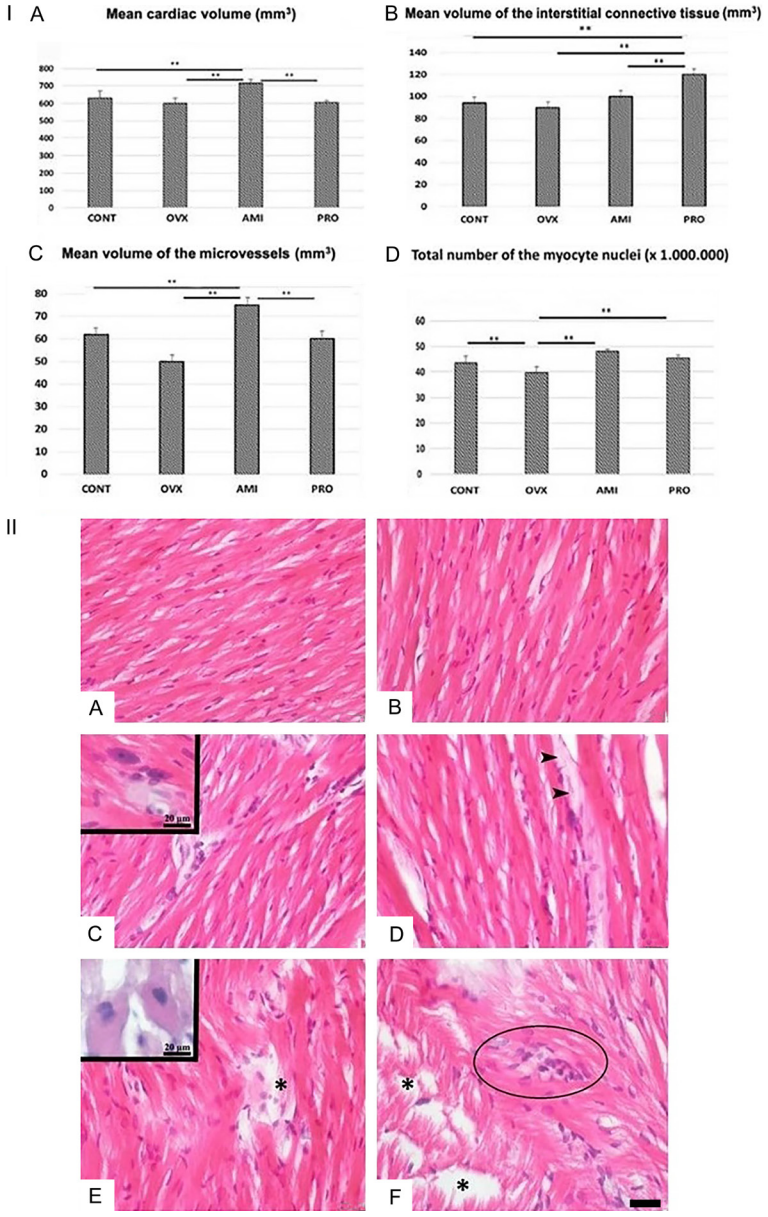

Figure 2. (IA-D) respectively shows the mean cardiac volume, mean volume of the interstitial connective tissue, mean volume of the microvessels, mean number of myocyte nuclei in all groups. ***P* value that is significant at the 0.01 level. (IIA-F) shows the histological structure of heart muscle by Hematoxylin and Eosin staining. (IIA) and (IIB) control rat's heart tissue with normal morphology; (IIC) and (IID) AMI-treated rats; (IIE) and (IIF) PRO-treated rats; asterisks, damaged myocytes; arrowheads, enlarged connective tissue sheets; circled areas, inflammatory cell infiltrates and insets show hypertophic myocytes with enlarged or hyperchromatic nuclei. Scale bars are 20 µm.

A one-way analysis of variance, specifically the Bonferroni post hoc test, was used to compare the groups and determine any variations in volumetric data and estimations of the cardiac myocyte number. Values are measured using the mean and standard error means (SEM), and any statistical values less than 0.05 were considered significant.

Results

Findings from stereological analysis

There were notable variations in the average heart volume between the AMI and PRO groups, as well as between the Control and AMI groups ($P < 0.01$) (**Figure 2IA**). The analysis of interstitial connective tissue volume showed a significant difference between the AMI and PRO groups ($P < 0.01$), the PRO and OVX groups, and the PRO and Control groups ($P < 0.01$) (**Figure 2IB**). When calculating the volume of micro-vessels, there was a noticeable difference between the AMI group and all other groups ($P < 0.01$) (**Figure 2IC**). The AMI group displayed the highest vessel volume. When comparing the total number of myocyte nuclei, there was no statistically significant difference between the AMI and PRO groups ($P > 0.05$). Nevertheless, notable distinctions were observed between the AMI and OVX groups, as well as between the AMI and CONT groups ($P < 0.01$) (**Figure 2ID**).

Histopathological view

During the categorization process for conventional light microscopy, the histological examination showed that cardiac muscle samples from the control rats exhibited a characteristic and healthy structure (**Figure 2IIA**, **2IIB**). On the other hand, the rats that had AMI and PRO treatment showed evident signs of harm to the structure of the heart muscle cells. This was marked by the disruption of cellular arrangement and the presence of inflammatory cells distributed or concentrated in certain areas.

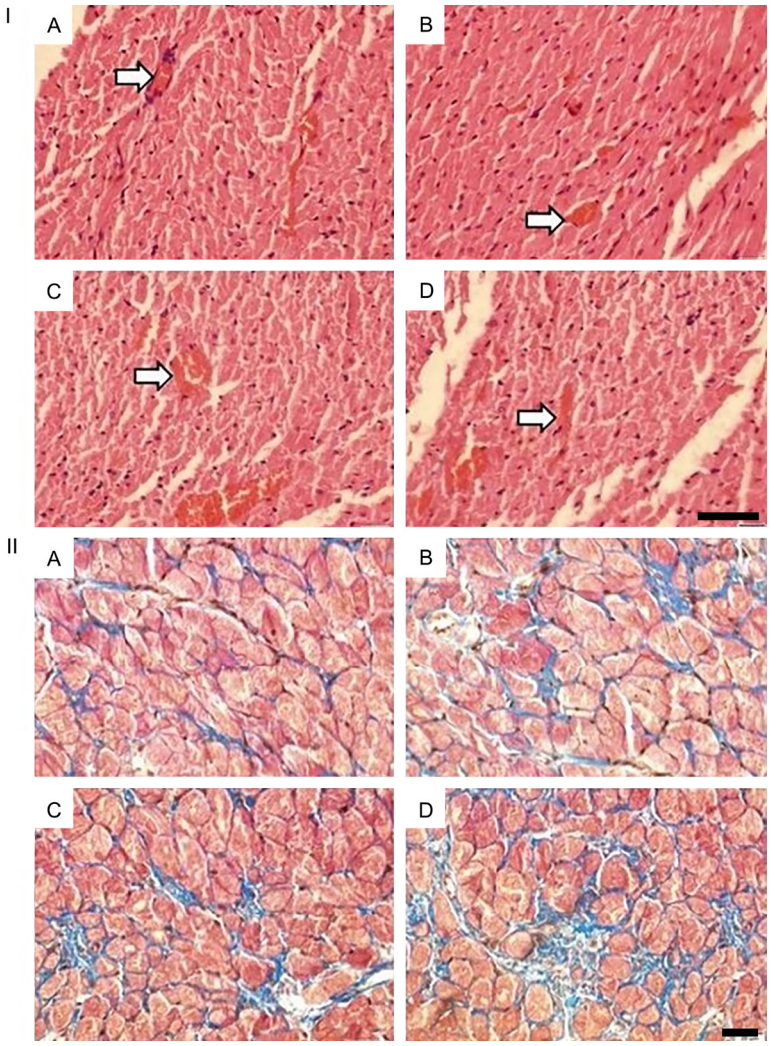

Figure 3. (IA-D) shows representative photomicrographs of the heart sections (left ventricular wall) on the transfers plan. Arrows show blood vessels in all groups. In the evaluation of vessel distributions, the AMI group has more and larger blood vessels when comparing with the other groups: (IA) Control. (IB) OVX. (IC) AMI. (ID) PRO. Stain: H&E; Scale bar, 200 μm. (IIA-D) also show photomicrographs of the heart sections (left ventricular wall) on the transfer plan. In the evaluation of interstitial connective tissue amounts by Masson's tricrome stain, the PRO group has more and larger interstitial connective tissue sheets when comparing with the other groups: (IIA) Control. (IIB) OVX. (IIC) AMI. (IID) PRO. Scale bar is 20 μm.

The infiltrates were composed primarily of lymphocytes, histiocytes, and plasma cells, with minimal presence of eosinophils and neutrophils. During the microscopic examination, we noticed enlarged myocytes with larger or more intensely stained nuclei in both groups (**Figure 2IIC-F** and insets). In the animals that received AMI treatment, multiple locations displayed enlarged connective tissue sheets (**Figure 2IID**). The heart tissues in the AMI-treated group displayed a more advanced histological structure in comparison to the rats treated with PRO. The group treated with AMI had a higher quantity of regions displaying cellular breakdown and a higher concentration of inflammatory infiltration foci, as depicted in **Figure 2IIE** and **2IIF**. When evaluating the small blood vessels in the heart wall, the group with acute myocardial infarction (AMI) shows a higher quantity and larger dimensions of blood vessels (**Figure 3IC**) compared to the other groups (**Figure 3IA**, **3IB**, and **3ID**). When analyzing the levels of interstitial connective tissue using Masson's trichrome stain, the PRO group showed higher amounts and wider areas of interstitial connective tissue compared to the other groups (**Figure 3IID**), as depicted in **Figure 3IIA-C**.

Expression of the C-Fos protein in the wall of the heart

The positivity of C-Fos in all groups was assessed by immunohistochemistry. Administrations of AMI and especially PRO to OVX rats led to an increase in C-Fos expression in the ventricle wall, as seen in **Figure 4IB**, **4ID**. Prominent signals were also identified in the ventricular septum and ventricular myocardium. The distribution of C-Fos in the heart exhibited non-uniformity. The ventricular myocardium exhibited a higher level of expression compared to the atrium. Within the ventricular region, the levels of C-Fos expression were significantly elevated in both the AMI and PRO groups compared to the Control and OVX groups, as demonstrated in **Figure 4IC**, **4ID**. The control group did not exhibit any expression of C-Fos, as shown in **Figure 4IA**. Immunohistochemical scoring results

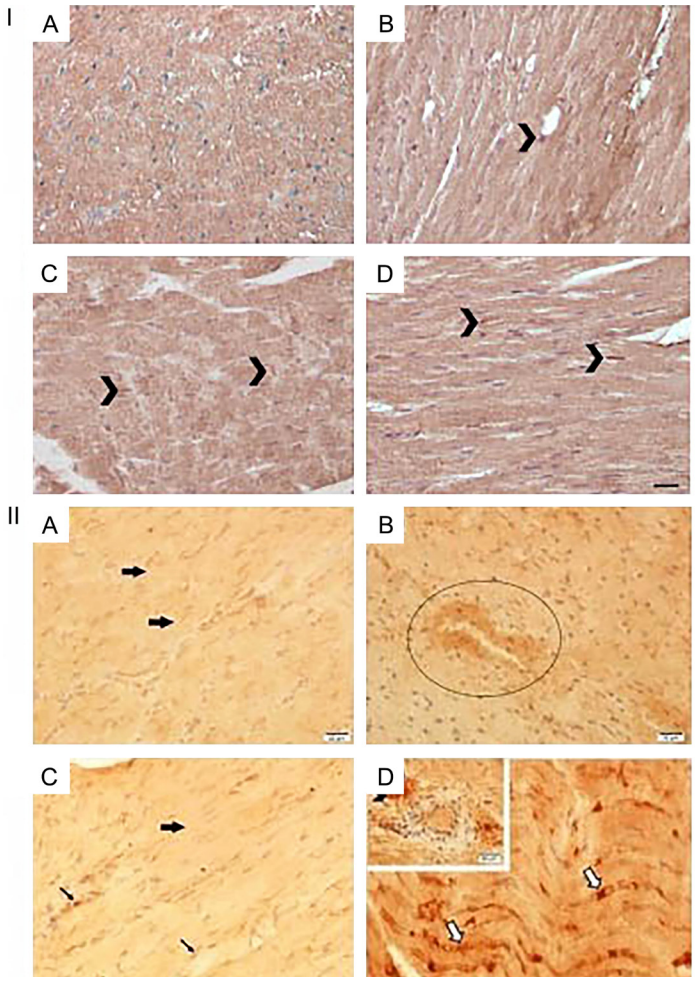

E

GROUPS	Positive cells (%)	Intensity	IHC score
CONT	3	0.24	0,72
OVX**	5	0.91	4,55
AMI**	6	1.17	7,02
PRO**	8	1.55	12,4

E

GROUPS	Positive cells (%)	Intensity	IHC score
CONT	2	0.42	0,84
OVX**	21	1,32	27,72
AMI**	16	1.86	29,76
PRO***	66	3.65	240,9

Figure 4. (IA-D) photomicrographs of c-fos immunoreactivity in the heart (left ventricular wall). Arrowheads show c-fos positive cells in each group. (IA) Control. (IB) OVX. (IC) AMI. (ID) PRO. Scale bar, 20 μm. (IIA-D) photomicrographs of NF-kB (P65) immunoreactivity in the heart (left ventricular wall). Thick arrows, thin arrows and white filled arrows show negative cells, weak positive cells and strong positive cells, respectively. Circled area indicates positive stained cells in the perivascular area and arrowhead in inset of (IID) shows positive stained nerve cell in the heart wall. (IIA) Control. (IIB) OVX. (IIC) AMI. (IID) PRO. Scale bars are 20 μm. (IE and IIE) exhibit immunohistochemical scoring tables of the groups for C-FOS and NF-kB antibodies respectively.

also confirmed the significant difference among the groups about C-Fos positivity; particularly in the ventricular region, C-Fos expression scores were significantly higher in the OVX, AMI and PRO groups, while no or minimal positive staining was observed in the control group. AMI and PRo groups shoved more postivity than OVX group (**Figure 4IE**).

Myocardial NF-kB expression

In order to identify possible inflammatory alterations in the heart wall, we assessed the level of NF-kB expression in cardiac myocytes from all heart samples (**Figure 4IIA-D**). Significant NF-kB expression was seen in both the cytosol and nucleus of many cardiomyocytes and nerve cells in cardiac samples from the PRO group (**Figure 4IID**, inset). **Figure 4IIA-C** demonstrates that a few cardiomyocytes in both the Control and AMI groups exhibited nuclei that were positive for NF-kB. Furthermore, the perivascular tissue of heart samples from rats in the OVX group exhibited NF-kB staining, as shown in **Figure 4IIB**. According to immunohistochemical scoring, NF-kB expression levels were significantly higher in the PRO group compared to the other groups. Also NF-kB positivity is higher in OVX, AMI and PRO groups then the CONT group (**Figure 4IIE**).

Discussion

Since postmenopausal depression is associated with reduced quality of life, impaired physical functioning, and increased suicidal ideation, it has become a major global public health concern. Therefore, determining the optimal treatment strategy is essential, taking into account both the risks of untreated depression and the potential benefits of therapy. Among cardiovascular risks, menopausal depression has been linked to increased severity of atherosclerosis [20]. Additionally, patients with depressive symptoms exhibit a higher risk of cardiovascular events and mortality from cardiovascular disease, independent of other established risk factors [21].

The menopausal period is characterized by distinct physiological changes, including an enhanced pro-inflammatory state, elevated inflammatory markers such as CRP and IL-8, and a decline in estrogen levels. Estrogen normally exerts cardioprotective and anti-inflammatory effects; thus, its reduction contributes to increased cardiovascular risk. Although continuous hormone therapy may be effective in managing menopausal depression, its use is limited due to elevated risks of venous thromboembolism, stroke, and breast cancer. Consequently, antidepressants with broad usage and favorable safety profiles have emerged as attractive alternatives. However, various studies have reported potential adverse effects of these agents, particularly in relation to cardiac function [9, 22].

While the cardiovascular and autonomic effects of SSRIs and TCAs at therapeutic doses have been widely explored, limited studies have assessed the morphological effects of amitriptyline (AMI, a TCA) and paroxetine (PRO, an SSRI) on cardiac tissue [23]. In the present study, we aimed to comparatively evaluate the potential cardiotoxic effects of these commonly prescribed antidepressants in an ovariectomized (OVX) rat model mimicking menopause. These findings are of particular relevance, as clinicians must consider cardiovascular risk profiles when selecting appropriate antidepressant therapy for postmenopausal patients. Furthermore, considering the elevated risk of sudden cardiac death or suicide in this population, histopathological data on antidepressant effects may also provide valuable information in forensic evaluations during autopsy.

This study is the first to investigate the histomorphometric and immunohistochemical effects of AMI and PRO on cardiac tissue in an OVX-induced menopausal model using the Cavalieri principle, physical dissection method, and immunohistochemical analysis of NF-κB and C-Fos expression. Stereological results demonstrated that PRO significantly increased total cardiac volume, primarily due to expansion of the interstitial connective tissue. The highest microvascular volume was observed in the AMI group. Both PRO and especially AMI reduced OVX-induced cardiomyocyte loss and increased cellular C-Fos immunoreactivity. Histological evaluation confirmed the stereological findings. AMI and PRO administration led to prominent myocardial architectural disturbances and cardiomyocyte damage, suggesting that long-term use of these antidepressants may impair cardiac function, possibly due to single-cell contractile dysfunction. PRO, in particular, caused more severe disruption in cellular architecture compared to AMI. Contrary to our results, several studies have reported cardioprotective effects of PRO. For example, PRO was found to attenuate cardiac injury biomarkers such as serum troponin I (Tn-I) and creatine kinase-MB (CK-MB), and to modulate markers of fibrosis, inflammation, and oxidative stress [24]. In another study, PRO enhanced β1-adrenergic receptor (ADRB1) sensitivity and attenuated cardiac hypertrophy by inhibiting GRK2 (G protein-coupled receptor kinase 2)-mediated ADRB1 desensitization and internalization in hypertensive models [25]. Similarly, AMI has been shown to exert beneficial effects on cardiac function in experimental settings, including reductions in left ventricular developed pressure (LVDP), dp/dt_max, and heart rate (HR), as well as a significant prolongation of the QRS interval [26]. In addition, AMI has been suggested to mediate cardioprotection through activation of the p38 MAPK signaling pathway [27].

We also examined C-Fos expression, an immediate-early gene upregulated in various pathophysiological processes, including drug exposure and inflammation. Although the mechanism underlying AMI- and PRO-induced C-Fos expression remained unclear, it is postulated that the abundance of catecholaminergic neu-

rons and noradrenergic innervation in the heart may lead to increased myocardial C-Fos expression following antidepressant administration [28]. This is consistent with previous findings showing rapid C-Fos upregulation in response to norepinephrine administration [29]. In our study, C-Fos immunoreactivity was observed in cardiomyocyte nuclei in both AMI- and PRO-treated OVX rats, while no C-Fos expression was detected in control group hearts, indicating that the observed response was specific to antidepressant treatment. C-Fos has commonly been used as a marker of neuronal activation [30], and PRO was previously shown to induce widespread Fos expression in adolescent and young adult rats [31]. Given the electrophysiological similarities between neurons and cardiomyocytes, immediate-early genes like C-Fos may serve as indicators of cardiac activity. Indeed, such genes are rapidly upregulated in response to stimuli such as ischemia-reperfusion injury, emotional stress, noradrenaline administration, immobilization, and drug exposure, all of which may be relevant in postmenopausal depression [12, 13].

In the current literature, some antidepressants have demonstrated protective effects against oxidative stress and redox imbalance beyond their pharmacological actions. In alignment with this, a gene expression study reported that PRO reduced β-myosin heavy chain (β-MyHC) and its associated myomiRs (miR-208 and miR-499) in a rat model of aortic regurgitation. PRO also downregulated the expression of BNP, a key biomarker of cardiac hypertrophy [32]. Additionally, AMI has been shown to activate TrkA/Akt phosphorylation and promote TrkA signaling, which protected cardiomyocytes against hypoxia/reoxygenation-induced apoptosis [33]. Although we did not directly investigate this mechanism in our study, it is plausible that AMI-induced increases in cardiomyocyte number and density occurred via TrkA/Akt pathway activation.

Furthermore, we assessed NF-κB expression, a protein complex that regulates the transcription of genes involved in immune and inflammatory responses. Upon activation, NF-κB triggers a cascade involving cytokines such as TNF-α, IL-1β, and IL-6 [34]. In this study, PRO administration led to increased NF-κB expression, particularly in the perivascular regions of the myocardium, indicating an inflammatory response. Conversely, some studies have shown that PRO attenuates IL-1β-induced pyroptotic activation and suppresses extracellular matrix catabolism via inhibition of NF-κB signaling. PRO has also been shown to downregulate RANKL-induced osteoclastogenesis [35]. Similarly, AMI was reported to suppress NF-κB-mediated cytokine expression, offering therapeutic potential for neuropathic pain [36].

The strength of the present study lies in the comprehensive evaluation of AMI and PRO on the heart using both stereological (Cavalieri and physical dissection methods) and immunohistochemical (NF-κB and C-Fos expression) techniques - performed for the first time in this context. However, the study has several limitations. First, we did not assess cardiac function through echocardiography, electrocardiography, or Holter monitoring following antidepressant treatment. Second, we were unable to measure biochemical or inflammatory markers indicative of cardiac stress or dysfunction. Third, while we analyzed C-Fos expression, we did not examine other immediate-early genes or signaling molecules relevant to the pathways affected by AMI and PRO.

Conclusion

It is clear from the findings in previous studies that menopausal depression and antidepressant therapies have a broad influence on the cardiovascular system. Therefore, when choosing an optimal treatment, the clinician must consider the risk-benefit ratio of any intervention. The results of this stereological and immunohistochemical study regarding the effects of SSRI and TCA drugs on the heart suggest that TCAs are safer than SSRIs in treatments. Thus, the undesirable outcomes of depression, such as systemic disorders and suicide, can be prevented through more confident therapies.

Disclosure of conflict of interest

None.

Address correspondence to: Dr. Emel Kurtoglu Ozdes, Department of Obstetrics and Gynecology, Faculty of Medicine, Kirklareli University, Kayali Campus, Kirklareli, Türkiye. E-mail: ekurtoglu0022@gmail.com; emel.ozdes@klu.edu.tr

References

[1] Kundakovic M and Rocks D. Sex hormone fluctuation and increased female risk for depression and anxiety disorders: from clinical evidence to molecular mechanisms. Front Neuroendocrinol 2022; 66: 101010.

[2] Morssinkhof MWL, van Wylick DW, Priester-Vink S, van der Werf YD, den Heijer M, van den Heuvel OA and Broekman BFP. Associations between sex hormones, sleep problems and depression: a systematic review. Neurosci Biobehav Rev 2020; 118: 669-680.

[3] El Khoudary SR, Aggarwal B, Beckie TM, Hodis HN, Johnson AE, Langer RD, Limacher MC, Manson JE, Stefanick ML and Allison MA; American Heart Association Prevention Science Committee of the Council on Epidemiology and Prevention; and Council on Cardiovascular and Stroke Nursing. Menopause transition and cardiovascular disease risk: implications for timing of early prevention: a scientific statement from the American heart association. Circulation 2020; 142: e506-e532.

[4] Fu P, Gibson CJ, Mendes WB, Schembri M and Huang AJ. Anxiety, depressive symptoms, and cardiac autonomic function in perimenopausal and postmenopausal women with hot flashes: a brief report. Menopause 2018; 25: 1470-1475.

[5] An SY, Kim Y, Kwon R, Lim GY, Choi HR, Namgoung S, Jeon SW, Chang Y and Ryu S. Depressive symptoms and suicidality by menopausal stages among middle-aged Korean women. Epidemiol Psychiatr Sci 2022; 31: e60.

[6] Xiang D, Liu Y, Zhou S, Zhou E and Wang Y. Protective effects of estrogen on cardiovascular disease mediated by oxidative stress. Oxid Med Cell Longev 2021; 2021: 5523516.

[7] Pasquali MA, Harlow BL, Soares CN, Otto MW, Cohen LS, Minuzzi L, Gelain DP, Moreira JCF and Frey BN. A longitudinal study of neurotrophic, oxidative, and inflammatory markers in first-onset depression in midlife women. Eur Arch Psychiatry Clin Neurosci 2018; 268: 771-781.

[8] Ungvari Z, Tarantini S, Yabluchanskiy A and Csiszar A. Potential adverse cardiovascular effects of treatment with fluoxetine and other selective serotonin reuptake inhibitors (SSRIs) in patients with geriatric depression: implications for atherogenesis and cerebromicrovascular dysregulation. Front Genet 2019; 10: 898.

[9] Coupland C, Hill T, Morriss R, Moore M, Arthur A and Hippisley-Cox J. Antidepressant use and risk of adverse outcomes in people aged 20-64 years: cohort study using a primary care database. BMC Med 2018; 16: 36.

[10] Aronow WS and Shamliyan TA. Effects of antidepressants on QT interval in people with mental disorders. Arch Med Sci 2020; 29: 727-741.

[11] Zhai LQ, Guo XJ, Li Z, Sun RF, Jin QQ, Liu MZ, Guo HL and Gao CR. Temporal changes in Egr-1 and c-fos expression in rat models of myocardial ischemia. Ann Palliat Med 2021; 10: 1411-1420.

[12] Bao Y, Qiao Y, Yu H, Zhang Z, Yang H, Xin X, Chen Y, Guo Y, Wu N and Jia D. miRNA-27a transcription activated by c-Fos regulates myocardial ischemia-reperfusion injury by targeting ATAD3a. Oxid Med Cell Longev 2021; 2021: 2514947.

[13] Ueyama T, Ishikura F, Matsuda A, Asanuma T, Ueda K, Ichinose M, Kasamatsu K, Hano T, Akasaka T, Tsuruo Y, Morimoto K and Beppu S. Chronic estrogen supplementation following ovariectomy improves the emotional stress-induced cardiovascular responses by indirect action on the nervous system and by direct action on the heart. Circ J 2007; 71: 565-73.

[14] Chelko SP, Asimaki A, Lowenthal J, Bueno-Beti C, Bedja D, Scalco A, Amat-Alarcon N, Andersen P, Judge DP, Tung L and Saffitz JE. Therapeutic modulation of the immune response in arrhythmogenic cardiomyopathy. Circulation 2019; 140: 1491-1505.

[15] Fiordelisi A, Iaccarino G, Morisco C, Coscioni E and Sorriento D. NFkappaB is a key player in the crosstalk between inflammation and cardiovascular diseases. Int J Mol Sci 2019; 20: 1599.

[16] Farkas AN, Marcott M, Yanta JH and Pizon AF. Bicarbonate refractory QRS prolongation and left bundle-branch block following escitalopram and lamotrigine overdose: a case report and literature review of toxic left bundle-branch block. J Clin Pharm Ther 2018; 43: 717-722.

[17] Sbolli M, Fiuzat M, Cani D and O'Connor CM. Depression and heart failure: the lonely comorbidity. Eur J Heart Fail 2020; 22: 2007-2017.

[18] Warille AA, Kocaman A, Elamin AA, Mohamed H, Elhaj AE and Altunkaynak BZ. Applications of various stereological tools for estimation of biological tissues. Anat Histol Embryol 2023; 52: 127-134.

[19] Ceccarelli S, Bei R, Vescarelli E, D'Amici S, di Gioia C, Modesti A, Romano F, Redler A, Marchese C and Angeloni A. Potential prognostic and diagnostic application of a novel monoclonal antibody against keratinocyte growth factor receptor. Mol Biotechnol 2014; 56: 939-52.

[20] Carranza-Lira S, Jimeno BLM and Ortiz SR. The relationship between carotid intima-media

thickness and cognitive function and depression in postmenopausal women. Prz Menopauzalny 2023; 22: 21-23.
[21] Inoue K, Beekley J, Goto A, Jeon CY and Ritz BR. Depression and cardiovascular disease events among patients with type 2 diabetes: a systematic review and meta-analysis with bias analysis. J Diabetes Complications 2020; 34: 107710.
[22] Jani BD, Mair FS, Roger VL, Weston SA, Jiang R and Chamberlain AM. Comorbid depression and heart failure: a community cohort study. PLoS One 2016; 11: e0158570.
[23] Hu MX, Milaneschi Y, Lamers F, Nolte IM, Snieder H, Dolan CV, Penninx BWJH and de Geus EJC. The association of depression and anxiety with cardiac autonomic activity: the role of confounding effects of antidepressants. Depress Anxiety 2019; 36: 1163-1172.
[24] Alonazi AS, Almodawah S, Aldigi R, Bin Dayel A, Alamin M, Almotairi AR, El-Tohamy MF, Alharbi H, Ali R, Alshammari TK and Alrasheed NM. Potential cardioprotective effect of paroxetine against ventricular remodeling in an animal model of myocardial infarction: a comparative study. BMC Pharmacol Toxicol 2024; 25: 99.
[25] Sun X, Zhou M, Wen G, Huang Y, Wu J, Peng L, Jiang W, Yuan H, Lu Y and Cai J. Paroxetine attenuates cardiac hypertrophy via blocking GRK2 and ADRB1 interaction in hypertension. J Am Heart Assoc 2021; 10: e016364.
[26] Hocaoğlu N, Murat N, Mıcılı SC, Aydın B, Ergür BU and Kalkan Ş. Correlation between amitriptyline-induced cardiotoxic effects and cardiac S100b protein in isolated rat hearts. Balkan Med J 2016; 33: 681-687.
[27] Lee SM, Hutchinson M, Staikopoulos V and Saint DA. Amitriptyline pharmacologically preconditions rat hearts against cardiac ischemic-reperfusion injury. Int J Cardiol 2015; 190: 353-9.
[28] Hernández-Gutiérrez S, Roque-Jorge J, López-Torres A, Díaz-Rosas G, García-Chequer AJ and Contreras-Ramos A. Role of sodium tetraborate as a cardioprotective or competitive agent: modulation of hypertrophic intracellular signals. J Trace Elem Med Biol 2020; 62: 126569.
[29] Lustberg D, Iannitelli AF, Tillage RP, Pruitt M, Liles LC and Weinshenker D. Central norepinephrine transmission is required for stress-induced repetitive behavior in two rodent models of obsessive-compulsive disorder. Psychopharmacology (Berl) 2020; 237: 1973-1987.
[30] Lee GJ, Kim YJ, Lee K and Oh SB. Patterns of brain c-Fos expression in response to feeding behavior in acute and chronic inflammatory pain condition. Neuroreport 2021; 32: 1269-1277.
[31] Karanges EA, Ramos L, Dampney B, Suraev AS, Li KM, McGregor IS and Hunt GE. Contrasting regional Fos expression in adolescent and young adult rats following acute administration of the antidepressant paroxetine. Brain Res Bull 2016; 121: 246-54.
[32] Omoto ACM, Moraes LN, Garcia GJF, Wechetti Junior IJ, Roscani MG, Carvalho RF and Fratucci de Gobbi IF. Glycemic index in the development of functional beverage. Eur Exp Biol 2018; 8: 19.
[33] Dai Y, Wang S, Li C, Chang S, Lu H, Huang Z, Zhang F, Yang H, Shen Y, Chen Z, Qian J and Ge J. Small molecule antidepressant amitriptyline protects hypoxia/reoxygenation-induced cardiomyocyte apoptosis through TrkA signaling pathway. Eur J Pharmacol 2017; 798: 9-15.
[34] Liu T, Zhang L, Joo D and Sun SC. NF-κB signaling in inflammation. Signal Transduct Target Ther 2017; 2: 17023.
[35] Zheng X, Qiu J, Gao N, Jiang T, Li Z, Zhang W, Gong Y, Hong Z and Hong H. Paroxetine attenuates chondrocyte pyroptosis and inhibits osteoclast formation by inhibiting NF-κB pathway activation to delay osteoarthritis progression. Drug Des Devel Ther 2023; 17: 2383-2399.
[36] Hwang Y and Kwon SY. Mode of action of amitriptyline against neuropathic pain via specific NF-kB pathway suppression. Pain Physician 2025; 28: E73-E79.